Hydrogeology Journal (2019) 27:2105–2119
https://doi.org/10.1007/s10040-019-01985-2

PAPER

Evaluation of water inrush from underlying aquifers by using a modified water-inrush coefficient model and water-inrush index model: a case study in Feicheng coalfield, China

Longqing Shi[1] · Mei Qiu[1,2] · Ying Wang[1] · Xingyue Qu[1] · Tianhao Liu[1]

Received: 3 June 2018 / Accepted: 8 May 2019 / Published online: 14 June 2019

Abstract

Water inrush from underlying aquifers seriously threatens mining of Permo-Carboniferous coal seams in many North China coalfields. To evaluate the risk of water inrush from underlying aquifers, a modified water-inrush coefficient method—using the water inrush coefficient (T) and geological structure index (G)—and a water-inrush index model (WII model) were proposed. The T_G model improved the traditional water-inrush coefficient method by quantifying the degree of geological structure development, considering three main controlling factors: G, aquifer water pressure (P) and aquitard thickness (M). The WII model was constructed to assess the risk of floor water inrush by the entropy weight method, which integrated six factors: G, P, M, the depth at which ground pressure creates a broken-rock zone (C_p), aquifer water yield property (Y), and percentage of brittle rock within the aquitard (B). Results from the engineering practice data analysis validated the T_G and WII models as operational tools to evaluate the risk of water inrush from an underlying aquifer. The comparative analysis of the predictions by these two models shows that the prediction accuracy of the WII model is 13% higher than that of the T_G model, and approximately 21% of the two model predictions are not in agreement. A more reasonable prediction was obtained with application of the T_G and WII models to Feicheng coalfield in Shandong Province to evaluate water inrush risk from the underlying aquifer, and the prediction offers guidance on different preventive measures against water hazards in the underlying Ordovician limestone in the different zones.

Keywords Water inrush · Mining · Risk evaluation · Water-inrush index model · China

Introduction

The primary North China coalfields are the Permo-Carboniferous coalfields distributed mainly in the Shanxi, Shandong, Henan, Hebei, Anhui, and Shaanxi Provinces. These coal seams are typically exploited via underground mining but at the risk of water inrush from underlying confined aquifers (Sun et al. 2015), especially those in Ordovician limestone. More than 200 water inrushes from Ordovician limestone have occurred in North China coalfields over the past 40 years, resulting in economic losses of more than 30 billion yuan and 1,300 deaths (Qiu et al. 2017a; Shi et al. 2015). Water problems in deep mining become increasingly serious as the mining depth increases (Gu et al. 2010); therefore, evaluating the water inrush risk from underlying aquifers is important to help control mine water hazards, and several evaluation methods have been developed over the past decades (Li et al. 2018; Wu et al. 2007). Among them, the water-inrush coefficient method has been widely used and plays an active role in assessing the risk of water inrush from underlying aquifers. However, due to the qualitative description of the degree of geological structure development and the few controlling factors considered, applications of the method are limited. Another important method is the

Electronic supplementary material The online version of this article (https://doi.org/10.1007/s10040-019-01985-2) contains supplementary material, which is available to authorized users.

✉ Mei Qiu
skdqiumei@126.com

[1] Shandong Provincial Key Laboratory of Depositional Mineralization & Sedimentary Minerals, College of Earth Sciences & Engineering, Shandong University of Science and Technology, Qingdao 266590, China

[2] State Key Laboratory of Mining Disaster Prevention and Control Co-founded by Shandong Province and the Ministry of Science and Technology, Shandong University of Science and Technology, Qingdao 266590, China

analytic hierarchy process (AHP) vulnerability index method proposed by Wu and Zhou (2008), which integrates multiple factors and has many potential advantages for assessing the probability of water inrush; however, the weights of the factors used in this method were assigned based on expert opinions, and included subjective judgments that vary for different individuals (Chang et al. 2007; Saaty 1980). Several mathematical methods have been introduced to assess the risk of water inrush, including the gray relational analysis, support vector machine (SVM), artificial neural network (ANN), random forest (RF), and unascertained measure theory, and these methods have enhanced the assessment of water inrush risk (Qiu et al. 2017b; Shi et al. 2017; Wang et al. 2012; Wu et al. 2008, 2017; Zhao et al. 2018); however, these methods have limitations for practical application. As an example, the gray relational analysis needs more water inrush cases to calculate the relative importance of each major controlling factor based on the geometric distance between the factors and the maximum water yield, but the maximum water yield does not well represent the risk of water inrush; the SVM model is limited because of its complex mathematical functions; the ANN model and RF can experience over learning, and their prediction processes are not well suited for field specialists because predicting a new case necessitates additional modeling and prediction; and in the unascertained measure theory (UMT), the constant weights of the factors are assigned based on subjective expert opinions.

In this study, a modified water-inrush coefficient method (T_G model) and a water-inrush index model (WII model) were proposed for comprehensive evaluation of the risk of water inrush from underlying aquifers into coal seams. The T_G model was developed by a comprehensive analysis of the water inrush coefficient (T) and geological structure index (G) based on water inrush cases, to improve the conventional water-inrush coefficient method that provides a fundamental basis for a water-inrush risk assessment. Meanwhile, the water-inrush index model (WII model), integrating multiple factors influencing water inrush, was established by the entropy weight method (EWM), which objectively assigns weights based on information given by an attribute database of factors, providing a more detailed scientific basis for water-inrush risk assessment. Data analysis of engineering practices was applied to verify the accuracy of the prediction results. A more reasonable prediction was accomplished by comprehensive application of these two model predictions to develop a zoning map of the water inrush risk, providing a more detailed scientific basis for safe production and control of water inrush.

Study area

The Feicheng coalfield is located in Feicheng City, Shandong Province in northern China, covering an area of approximately 120 km^2 that includes seven coal mines: Chazhuang, Guozhuang, Baizhuang, Taoyang, Dafeng, Caozhuang, and Yangzhuang mines from west to east. The coalfield region has a semiarid climate and warm temperatures. The average annual precipitation is approximately 662 mm, and the average annual evaporation is 442 mm. The overall geological structure of the coalfield is a monocline dipping to the north, accompanied by small folds. The dip angle is mainly 5–10°, but locally can be more than 20°. The faults are well developed with the main striking NE, NNE, NW, and ENE (Fig. 1).

According to outcrop observations and drilling data, the strata in the Feicheng coalfield are of the Ordovician system (O), Carboniferous system (C), Permian system (P), Paleogene system (E), and Quaternary system (Q), from oldest to youngest. The coal-bearing strata in the Feicheng coalfield originated during the Permo-Carboniferous period. These strata include five primary mineable seams: No. 3_1 in the Shanxi Formation (F) and Nos. 7, 8, 9, and 10_2 coal seams in Taiyuan F (from top to bottom). Coal seams Nos. 8, 9, and 10_2 are threatened by underlying limestone aquifers, especially the fifth limestone aquifer of Taiyuan F and the Ordovician karst limestone aquifer. During mining of the No. 8 coal seam, 29 water inrushes from the fifth limestone aquifer and one extra-large-scale, two large-scale, and one medium-scale water inrushes from the Ordovician limestone aquifer occurred. The Ordovician limestone aquifers have abundant water with a large thickness of approximately 800 m and a high hydraulic pressure exerted by the upper confining bed. With increasing mining depth, the hydrogeological conditions become more complicated, and safe extraction of the No. 8 coal seam is increasingly threatened by the underlying Ordovician limestone aquifer.

Methodology

Modified water-inrush coefficient model

Water inrush coefficient

The water-inrush coefficient method was put forward for assessing the risk of water inrush from underlying aquifers in the 1960s and is stipulated in the "Regulations for Coal Mine Water Prevention and Control, China" (Ministry of Coal Industry 2009) which was modified several times. According to the latest Coal Mine Water Control Rules (Ministry of Coal Industry 2018), the water inrush coefficient is expressed as Eq. (1).

$$T = \frac{P}{M} \tag{1}$$

where T is the water inrush coefficient, indicating the bearing pressure of the unit aquitard thickness (MPa/m); P is the aquifer water pressure sustained by the coal seam floor (MPa),

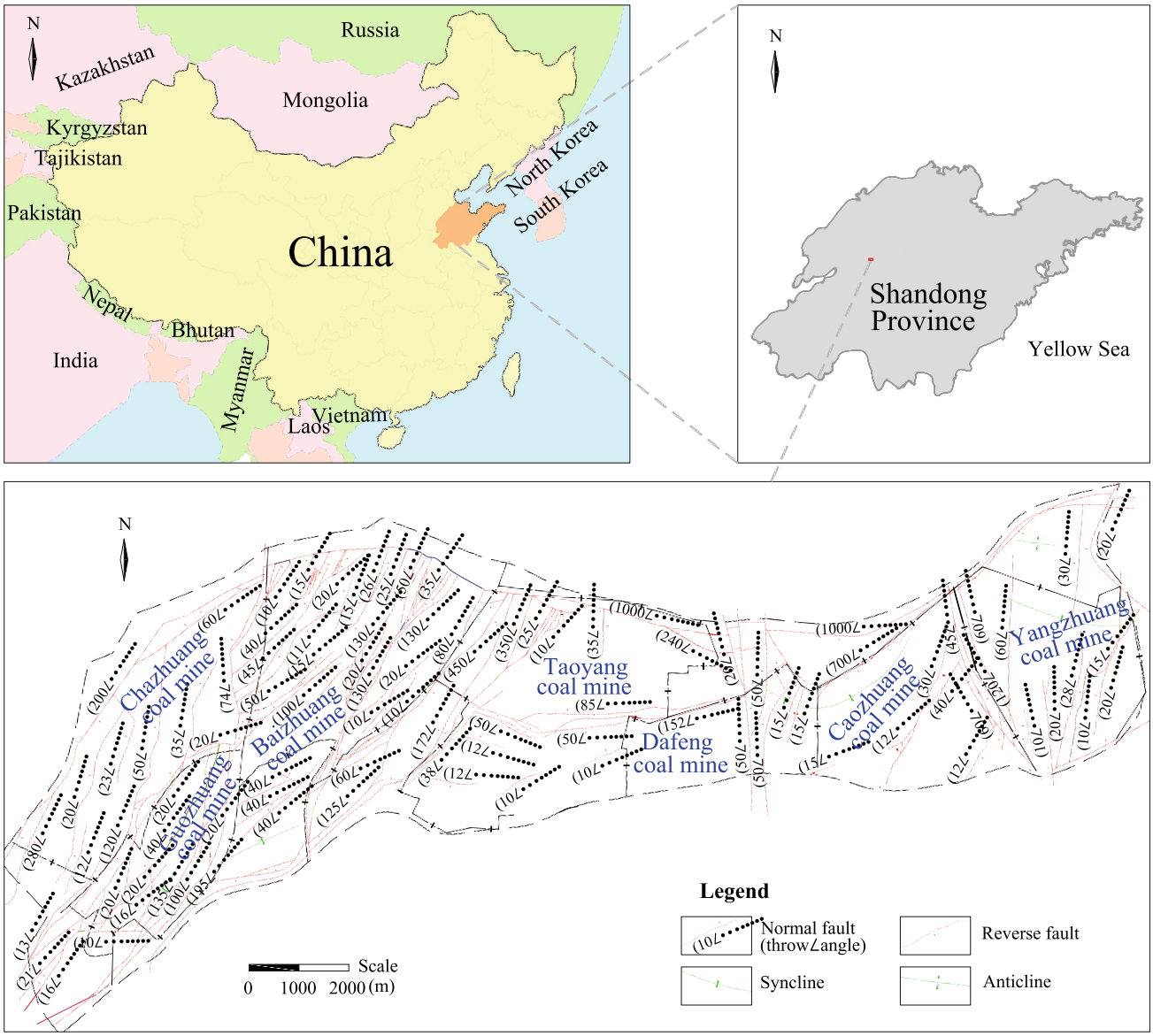

Fig. 1 Location of the study area in Shandong Province, China, and the geological structure of the Feicheng coalfield

which was calculated according to the elevation difference between the aquifer water level and the Ordovician limestone top in this study; and M is the aquitard thickness (m) which is defined as the distance between coal floor and aquifer floor, and the data of M was acquired from the geo-exploration. The data of P and M were processed using the SURFER software and interpolated with the Kriging function interpolation technique to create a contour map, respectively. The study area was divided into 500 m × 500 m grids by using longitudinal and latitudinal lines, and the values of P and M in each grid unit were obtained by interpolation of the established contour maps—Table S1 of the electronic supplementary material (ESM). Finally, the water inrush coefficient was computed using Eq. (1) in each grid unit, and the contour map of the water inrush coefficient was constructed using the Kriging function interpolation technique (Fig. 2).

The Coal Mine Water Control Rules (Ministry of Coal Industry 2018) gives the critical value of water inrush. Water inrushes tend not to occur if $T < 0.06$ MPa/m in simple structural areas and $T < 0.10$ MPa/m in complex structural areas. The water-inrush coefficient method is simple and practical; therefore, it is widely applied and has an active role in assessing the risk of water inrush from underlying aquifers in China. However, the qualitatively described simple and complex structural areas are difficult to distinguish, resulting in subjective judgments that vary for different individuals; therefore, a modified water-inrush coefficient model should be proposed based on T and geological structure development degree.

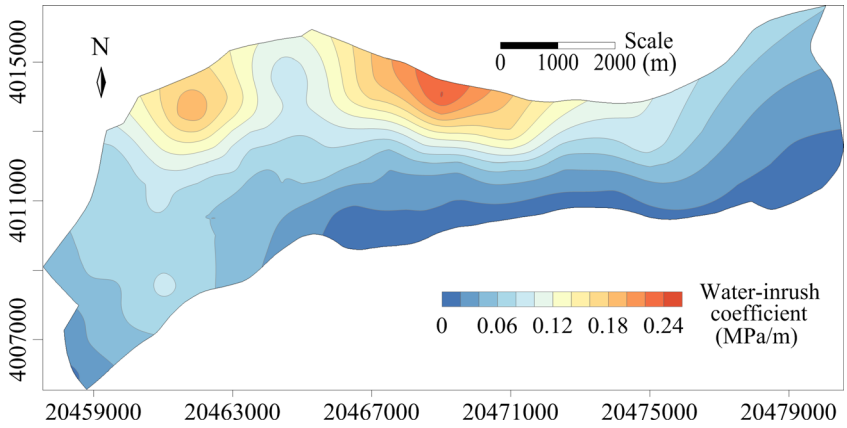

Fig. 2 Contour map of the water inrush coefficient (T)

Geological structure development degree

First, the degree of geological structure development, which has a significant influence on water inrush, was quantified. In the Feicheng coalfield, the faults associated with folds are well developed (Fig. 1), revealed by 3D-seismic exploration, geo-exploration, and roadway and workface extractions. Fault throw and strike length can reflect fault intensity, which is very closely related to water inrush (Qiu et al. 2017b). Faults with large fault throws and long lengths decrease the performance of an aquitard in preventing floor water inrush. Faults can also decrease the distance between coal seams and aquifers and even cause coal seams to connect with aquifers. The fault intensity index (I_{FI}) is defined as (Xu et al. 1991):

$$I_{FI} = \frac{\sum_i^n l_i h_i}{S} \tag{2}$$

where I_{FI} is the fault intensity index, h_i is the ith fault throw (m), l_i is the ith fault's strike length (m), S is the area with a grid unit size of 500 m × 500 m (m^2), and $i = 1, 2, \ldots, n$, where n is the total number of faults in each grid unit. The values of the fault throw and strike length of each fault were determined according to the map of the geological structure of the Feicheng coalfield (Fig. 1), which was drawn based on 3D-seismic exploration, geo-exploration, and roadway and workface extractions data, and then the I_{FI} value was obtained for each grid unit. The contour map of the fault intensity index was established by SURFER software using the Kriging function interpolation technique, as shown in Fig. 3.

The other important fault factor is the density of the fault intersections and endpoints (D_{FIE}), which reflects the extent of coal floor strata fracturing (Wu et al. 2011). Rock is more crushed and fractures are more developed at the intersections and endpoints of faults where ground stress tends to concentrate. The density of fault intersections and endpoints is the sum of all the intersections and endpoints of all faults divided by the grid unit area and is calculated by Eq. (3) (Wu et al. 2011):

$$D_{FIE} = \frac{n}{S} \tag{3}$$

where D_{FIE} is the density of fault intersections and endpoints ($/m^2$), n is the total number of fault intersections and endpoints of all faults in each grid unit, and S is the area of the grid unit (m^2). The number of fault intersections and endpoints in each 500 m × 500 m grid unit was counted according to the map of the geological structure of the Feicheng coalfield (Fig. 1), and the D_{FIE} value was obtained for each grid unit. The contour map of the density of fault intersections and endpoints was established by SURFER software and shown in Fig. 4.

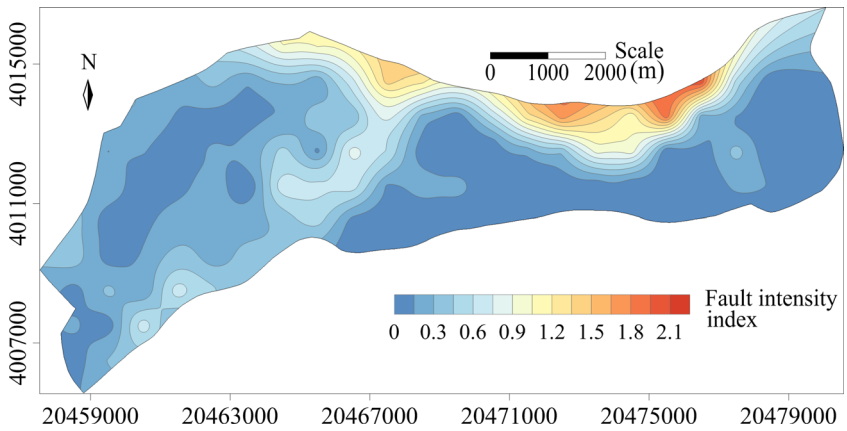

Fig. 3 Contour map of the fault intensity index (I_{FI})

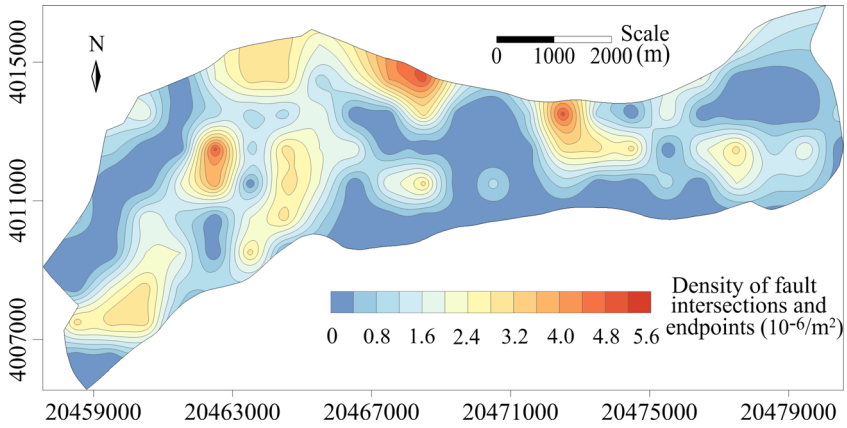

Fig. 4 Contour map of the density of fault intersections and endpoints (D_{FIE})

The density of the fold-axis length (D_{FAL}) is the main factor describing the fold distribution. Along the length of the fold axis, fractures are well developed which are destructive to the integrity and continuity of the coal floor strata. Even small folds can create water-inrush risk zones. D_{FAL} is calculated by the following equation (Qiu 2016).

$$D_{FAL} = \frac{\sum_t^r L_t^2}{S} \tag{4}$$

where L_t is the tth fold's axis length in a grid (m); S is the area with a grid unit size 500 m × 500 m (m^2); and $t = 1, 2, \ldots, r$, where r is the total number of folds in each grid unit. The length of each fold axis was counted to calculate D_{FAL} for each 500 m × 500 m grid unit, and the contour map of the fold-axis length density was established by SURFER software, as shown in Fig. 5.

After collecting each factor, the data should be normalized by relativization to make the data comparable and statistically significant because the different dimensions of the factors could unduly influence the evaluation results (Ma 2003), as shown in (Wu et al. 2011):

$$A_i = a + \frac{(b-a) \times (x_i - \min(x_i))}{\max(x_i) - \min(x_i)} \tag{5}$$

where A_i is the normalized data; a and b are the lower and upper limits of normalization, respectively ($a = 0.1$, and $b = 0.9$); x_i is the original data before normalization; and $\min(x_i)$ and $\max(x_i)$ are the minimum and maximum values.

Finally, a geological structure index (G) was established to quantify the degree of geological structure development based on normalized I_{FI}, D_{FIE} and D_{FAL} values. Based on practical experience, the field specialists (Jinwei Ma, Xiujun Zhang) and professors (Yongkui Shi, Jiuchuan Wei) working with the mines in the coalfield assigned weights of $P_1 = 0.5$, $P_2 = 0.2$, and $P_3 = 0.3$ to I_{FI}, D_{FIE} and D_{FAL}, respectively. The geological structure index (G) was calculated as:

$$\begin{aligned} G &= P_1 \cdot I_{FI}' + P_2 \cdot D_{FIE}' + P_3 \cdot D_{FAL}' \\ &= 0.5 I_{FI}' + 0.2 D_{FIE}' + 0.3 D_{FAL}' \end{aligned} \tag{6}$$

where G is the geological structure index; I_{FI}', D_{FIE}' and D_{FAL}' are normalized values of the fault intensity index, quantity of fault intersections and endpoints, and fold-axis density, respectively, and P_1, P_2, and P_3 are the weights of the aforementioned factors.

Based on the geological structure index model, the value of the geological structure index in each 500 m × 500 m grid unit was obtained by using Eq. (6), and the contour map of the geological structure index was established by SURFER software, as shown in Fig. 6. The geological structure index is

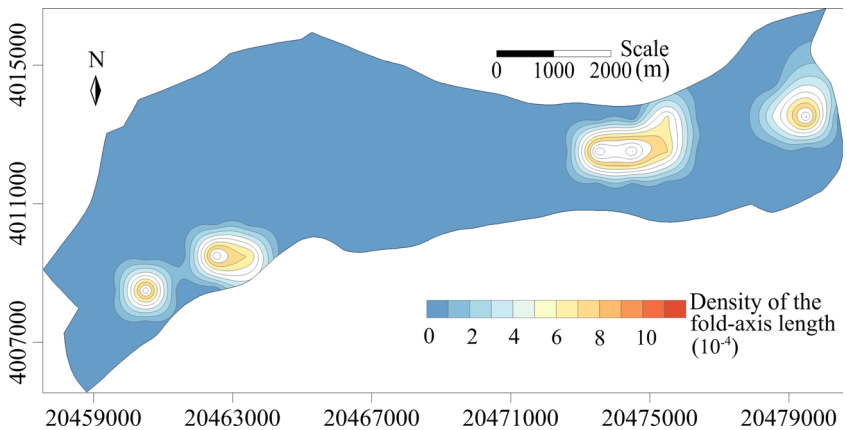

Fig. 5 Contour map of the fold-axis length density (D_{FAL})

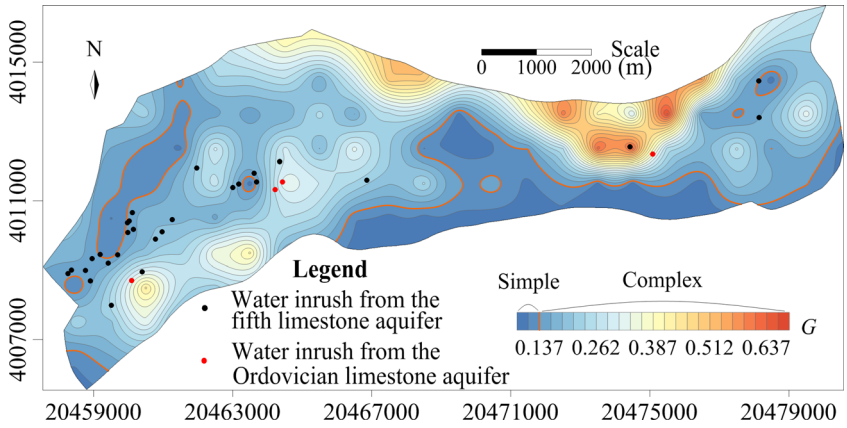

Fig. 6 Contour map of the geological structure index (G)

0.087–0.666 in the study area, indicating large changes in the degree of geological structure development. A larger geological structure index value indicates a more complicated geological structure development degree.

To distinguish the simple and complex structural areas, the values of the geological structure index at 33 water inrush points were gathered (Fig. 6) and a histogram of the water-inrush point distribution is shown in Fig. 7. The geological structure index values of all water inrush points are greater than 0.137, indicating that the geological structure is the main factor controlling water inrush in the region where $G \geq 0.137$. Therefore, $G = 0.137$ was taken as the partition threshold, and the structure development degree was divided into two distinct zones (Fig. 6):

1. Simple structural areas: $G < 0.137$, in only small parts of the study area, mainly distributed in the southern area and a small part of the western area
2. Complex structural areas: $G \geq 0.137$, in two-thirds of the study area mainly distributed in the northern, eastern, and western areas of the study area

T_G evaluation model

According to the Coal Mine Water Control Rules (Ministry of Coal Industry 2018), the modified water-inrush coefficient model for the risk evaluation of water inrush was established by comprehensive analysis of T and G and called the T_G evaluation model, or simply "T_G", as shown in the following:

$$T\_G = \begin{cases} T < 0.06 \ \text{(safe)} \\ 0.06 \leq T < 0.10, \text{and} \begin{cases} G < 0.137 \ \text{(safe)} \\ G \geq 0.137 \ \text{(dangerous)} \end{cases} \\ T \geq 0.10 \ \text{(dangerous)} \end{cases} \quad (7)$$

As shown in Eq. (7), the water-inrush risk evaluation rules based on the T_G evaluation model are as follows: (1) the risk of water inrush is classified as safe when one of the following occurs: $T < 0.06$ MPa/m or $0.06 \leq T < 0.10$ MPa/m and $G < 0.137$; and (2) the risk of water inrush is classified as dangerous when one of the following occurs: $T \geq 0.10$ MPa/m or $0.06 \leq T < 0.10$ MPa/m and $G \geq 0.137$.

Water-inrush index model

Factors

The modified water-inrush coefficient model considers three main factors: aquifer water pressure (P), aquitard thickness (M), geological structure index (G). The aquifer water yield property (Y), mechanical strength of an aquitard denoted by the percentage of brittle rock within the aquitard (B), and the depth at which a zone of broken rock forms under the pressure associated with mining—hereafter, the 'depth of broken rock created by ground pressure' (C_p)—were neglected. Therefore, a water-inrush index model that integrates six factors, including P, M, C_p, G, Y, and B, was then proposed to improve the prediction results based on the entropy weight method.

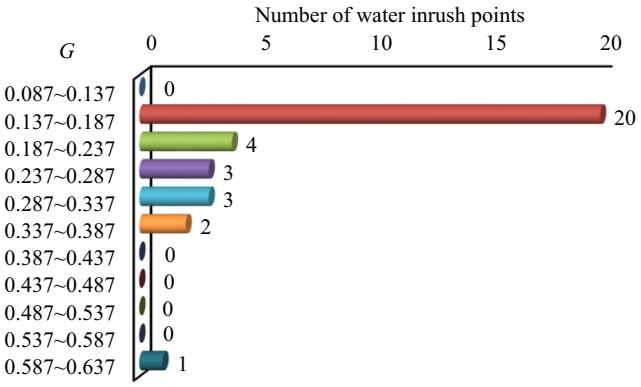

Fig. 7 Histogram of the distribution of water inrush points

1. *Aquifer water pressure (P)*. Water inrush from an underlying aquifer results from pressure constantly acting on the upper confining bed of the aquifer below (Wu et al. 2011). As aquifer water pressure increases, coalmines are at a higher risk of water inrush. The data source of the aquifer water pressure is the same as that for the *P* in Eq. (1), and includes the same calculation method.
2. *Aquitard thickness (M)*. Aquitards act as geologic barriers and can prevent water in an underlying aquifer from flowing into mines. One of the factors indicating the water-resistant ability of an aquitard is aquitard thickness. A thicker aquitard provides better protection. The data source of the aquitard thickness is the same as that of the *M* in Eq. (1).
3. *Depth of broken rock created by ground pressure (C_p)*. During mining, the ground pressure caused by mining inevitably damages the surrounding floor rock. C_p is defined as the distance between the coal seam floor and the deepest boundary of the floor rock damaged by the ground pressure. A larger C_p results in a greater relative risk of water inrush. The C_p value can be calculated with reference to *Pillar design and mining regulations under buildings, water, rails and major roadways* (National Bureau of Coal Industry of China 2000), by using the following empirical formula:

$$C_p = 0.0085H + 0.1665\alpha + 0.1079L - 4.3579 \quad (8)$$

where C_p indicates the depth of broken rock created by ground pressure (m); H indicates the mining depth (m), which was acquired from 3D-seismic exploration, geo-exploration, and roadway and workface constructions; α indicates the dip angle of the No. 8 coal seam (°), which was acquired from geo-exploration, and roadway and workface constructions; and L indicates the mining width of the mining face (m), which was acquired from actual mining width where the No. 8 coal seam was mined, and which was 105 m where the No. 8 coal seam has not been mined.
4. *Geological structure index (G)*. The geological structure is the key to water inrush from the underlying aquifer. The geological structure index calculated by Eq. (6) was adopted for water inrush forecasting.
5. *Aquifer water yield property (Y)*. The aquifer water yield property is a key factor in coal floor water inrush and indicates the productivity of an aquifer. The yield is directly reflected by the unit water inflow, which was obtained from pumping tests of hydrogeological boreholes.
6. *Percentage of brittle rock within the aquitard (B)*. The percentage of brittle rock within the aquitard is another factor affecting the water-resistant ability of the aquitard, which was calculated by dividing brittle rock thickness by the aquitard thickness based on the geo-exploration data. Brittle rock tends to have a higher water-resisting ability than plastic rock (Li 2000; Meng et al. 2012); thus, the greater the percentage of brittle rock within the aquitard, the lower the probability of water bursts (Wu and Zhou 2008).

The data of *P*, *M*, C_p, *G*, *Y*, and *B* were processed using the SURFER software and interpolated with the Kriging function interpolation technique to create six thematic maps, shown in Fig. 8.

Data normalization and the database

The values of six main factors including *P*, *M*, C_p, *G*, *Y*, and *B* were collected in 479 grid units of 500 m × 500 m and four water inrush points by interpolation of the established thematic maps (Fig. 8). Then, normalization by relativization was carried out to make the data comparable and statistically significant using the following equation (Qiu et al. 2017b):

$$A_i = \begin{cases} a + \dfrac{(b-a) \times (x_i - \min(x_i))}{\max(x_i) - \min(x_i)}, \text{where } x \text{ is a positive factor} \\ a + \dfrac{(b-a) \times (\max(x_i) - x_i)}{\max(x_i) - \min(x_i)}, \text{where } x \text{ is a negative factor} \end{cases} \quad (9)$$

In this paper, the positive factors are *P*, C_p, *G*, and *Y*, which indicate a higher risk when the factor value is larger, and the negative factors are *M* and *B*, which indicate a lower risk when the factor value is larger. After data normalization, an attribute database of the six normalized main factors (*P*′, *M*′, C_p′, *G*′, *Y*′, and *B*′) was established for constructing the evaluation model of water inrush index by EWM (Table S1 of the ESM).

Evaluation model of water inrush index by the entropy weight method (EWM)

The concept of entropy in information theory was proposed by Shannon (1948) and then widely employed in engineering fields. Entropy is a measure of the degree of uncertainty represented by a discrete probability distribution, which objectively weights factors based on the information given by the attribute database of the six main factors (Table S1 of the ESM) as a feasible scientific method. The greater the difference between factors, the smaller the entropy, indicating a larger weight factor. Four steps were followed to determine the objective weights of the six main factors (Wang et al. 2018):

1. *Construction of the decision matrix* (Wang et al. 2018).

$$R = \begin{pmatrix} x_{11} & \cdots & x_{1n} \\ \vdots & \ddots & \vdots \\ x_{m1} & \cdots & x_{mn} \end{pmatrix} \quad (10)$$

where x_{ij} is the value of the *i*th evaluated-sample *j*th factor in Table S1 of the ESM; $i = 1, 2, \ldots, m$; $j = 1, 2, \ldots, n$; and

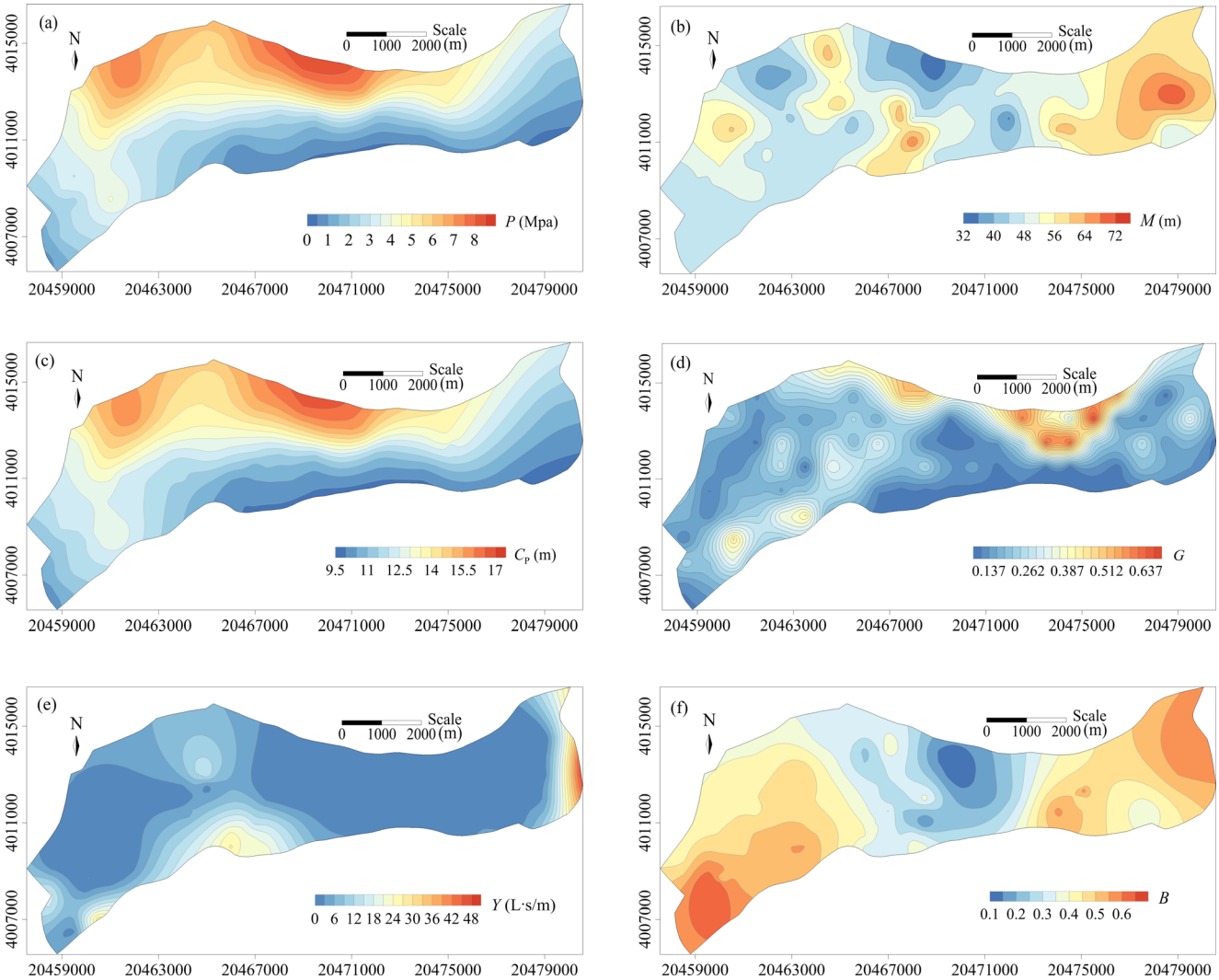

Fig. 8 Thematic map of the main water inrush factors: **a** aquifer water pressure, **b** aquitard thickness, **c** depth of broken rock created by ground pressure, **d** geological structure index, **e** aquifer water yield property, and **f** percentage of brittle rock within the aquitard

m and n are the total number of evaluated samples and factors, respectively. In this paper, $m = 483$ and $n = 6$.

2. *Calculation of the project outcomes,* p_{ij} (Wang et al. 2018).

$$p_{ij} = \frac{x_{ij}}{\sum_{i=1}^{m} x_{ij}} \tag{11}$$

3. *Calculation of the entropy of the jth factor* (Wu et al. 2015).

$$E_j = -\frac{1}{\ln m} \sum_{i=1}^{m} p_{ij} \ln p_{ij} \tag{12}$$

4. *Establishment of the entropy weight of the jth factor* (Huang et al. 2017).

$$\omega_j = \frac{1 - E_j}{\sum_{j=1}^{n} (1 - E_j)} \tag{13}$$

In this study, a 483 × 6 decision matrix was established for the following calculations based on the attribute database of the six normalized main factors (P', M', C_p', G', Y', and B'; Table S1 of the S1). Following the above steps, the entropy E and entropy weight ω of each factor were obtained as shown in Table 1. The weights of P, M, C_p, G, Y, and B were 0.169, 0.046, 0.177, 0.195, 0.293, and 0.120, respectively.

The water inrush index (WII) can be defined as the comprehensive criterion of floor water-inrush risk of an evaluated sample. As for an evaluated sample, every main factor acts together and forms the comprehensive criterion. The water inrush index for each evaluated sample can be expressed as follows:

$$\mathrm{WII} = \sum_{j=1}^{n} \omega_j \cdot f_j(x, y) \tag{14}$$

where WII is the water inrush index; n is the number of main factors of water inrush considered, which is six in this paper;

Table 1 The values of entropy E and entropy weight of each main factor of water inrush

Factor	P	M	C_p	G	Y	B
Entropy E	0.984	0.996	0.983	0.981	0.972	0.989
Entropy weight ω	0.169	0.046	0.177	0.195	0.293	0.120

$j = 1, 2, \ldots, n$ indicates the sequence number of the main factors; and $f_j(x, y)$ is the normalized value of the jth factor at the geographic location (x, y) of the evaluated sample. Based on the attribute database of the six normalized main factors and the weights listed in Table 1, the risk evaluation model for floor water inrush of the No. 8 coal seam in the Feicheng coalfield was ultimately established as follows:

$$\begin{aligned} \mathrm{WII} = \sum_{j=1}^{n} \omega_j \cdot f_j(x,y) = {} & 0.169P' + 0.046M' \\ & + 0.177C_p' + 0.195G' \\ & + 0.293Y' + 0.120B' \end{aligned} \quad (15)$$

where P', M', C_p', G', Y', and B' are the normalized factors P, M, C_p, G, Y, and B, respectively.

The values of WII for areas where water inrush occurred and areas where safe mining was achieved were calculated to determine the partition threshold, and using this threshold, the risk of water inrush can be classified into two zones. The partition threshold is defined as follows:

$$T_{s\text{-}d} = (\max(\mathrm{WII_s}) \cdot \min(\mathrm{WII_d}))^{1/2} \quad (16)$$

where $T_{s\text{-}d}$ is the partition threshold that separate safe areas and dangerous areas; $\mathrm{WII_s}$ indicates the value of the water inrush index in the area where safe mining was achieved; and $\mathrm{WII_d}$ indicates the value of the water inrush index in the area where water inrush occurred. Thus, the water inrush risk from an underlying aquifer can be divided into two zones:

- Zone I in which $\mathrm{WII} < T_{s\text{-}d}$, indicating a safe scenario
- Zone II in which $\mathrm{WII} \geq T_{s\text{-}d}$, indicating a dangerous scenario

Results and discussion

Results

The values of T and G were calculated for each 500 m × 500 m grid unit. Based on the T_G evaluation model, the risk-evaluation grade was realized. Meanwhile, a water-inrush risk zone map based on the T_G model was constructed by integrating the information storage layers of the water inrush coefficient (Fig. 2) and geological structure index (Fig. 6) into one layer (Fig. 9). As shown in Fig. 9, the study area was divided into two zones based on the T_G model: safe and dangerous. Among these, dangerous zones with high water inrush potential accounted for 65% of the total area, and these zones are located in the western and northern areas of the study area. Especially in the northwest part of the study area, water inrushes are most likely to occur with bigger values of T and G, because the water pressure is high and the degree of geological structure development is complicated. The safe zones are mainly located in the southern part and small southwestern part of the study area where the water pressure is low and the degree of geological structure development is simple.

The value of WII was obtained for each 500 m × 500 m grid unit based on the water-inrush index model. All grid unit data were then processed by using Surfer software. The WII contour model map was constructed by using the Kriging function interpolation technique, as shown in Fig. 10. The water inrush risk of the No. 8 coal seam from the underlying Ordovician limestone aquifer expressed by WII ranges from 0.164 to 0.587. The higher the WII value, the greater the probability of water inrush. To determine the partition threshold for the dangerous and safe zones, the values of WII were calculated for the four water inrush points and 70 safe mining

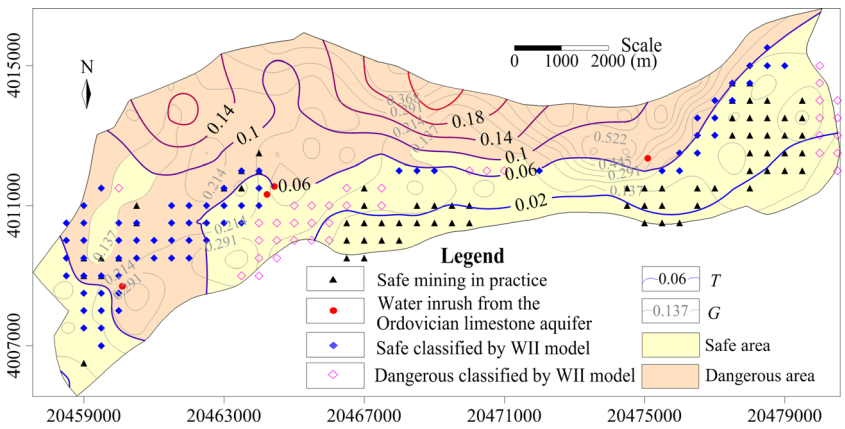

Fig. 9 Water-inrush risk zone by the T_G model

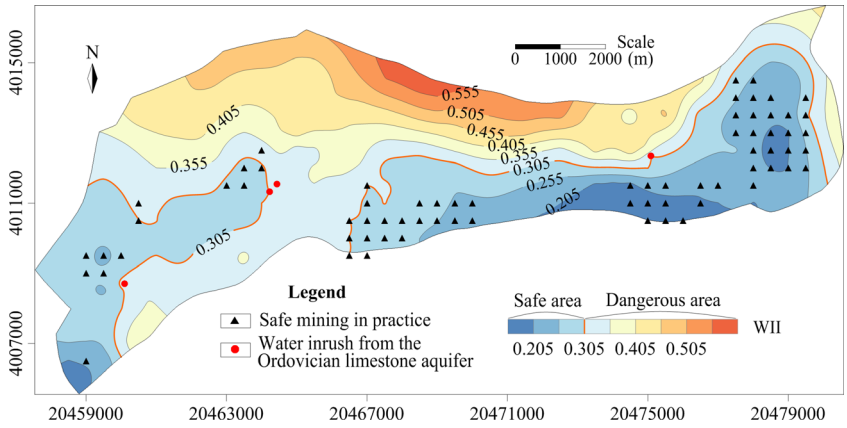

Fig. 10 Water-inrush risk zone by the WII model

units (Table 2). The minimum value of WII for the four water inrush points was 0.306, and the maximum value of WII for the four water inrush points was 0.305 (excluding two outliers in Nos. 58 and 155 in Table 2). Thus, the partition threshold was calculated based on Eq. (16) as $T_{s\text{-}d} = 0.305$, and the risk of water inrush in the No. 8 coal seam from the underlying aquifer was classified into two zones (Fig. 10):

- Zone I: WII < 0.305, safe zone with a small likelihood of water inrush, mainly located in the eastern, southern, and southwest parts of the study area.
- Zone II: WII ≥ 0.305, dangerous zone where water inrushes are most likely to occur, mainly in small parts of the western, northwestern, and northern areas of the study area. This risk zone occupies approximately 58% of the total area.

Validation of the predictions

Validation is crucial to verify results; therefore, to verify the accuracy of the prediction results based on the *T_G* and WII models proposed in this paper, validation tests were carried out by comparing the prediction results with practical results. A total of 74 test samples, including four water inrush points from the Ordovician limestone aquifer and 70 safe mining units, were collected to test the prediction results. The results predicted by these two methods and the practical results obtained for the 74 test samples are shown in Table 2.

Figure 11 shows the comparison between the prediction results from the *T_G* model and the practical outcomes for the 74 test samples. Among these 74 test samples, 11 samples were safe for mining but were classified as dangerous, and one sample with water inrush occurred but was classified as safe by the *T_G* model. Thus, the verification rate of the *T_G* model prediction was 84%.

Figure 12 illustrates the comparison between the results predicted by the WII model and the practical outcomes for the 74 test samples. The predicted results for four water inrush points by the WII model were in agreement with the actual results. Only two samples that are safe in reality were predicted to be dangerous based on the WII model; thus, the verification rate of the WII model prediction was up to 97%, indicating that the predicted results align well with the actual results.

Comparative analysis, and comprehensive application of the two methods

Based on the validation of the prediction results from these two methods, the accuracy of the methods is at least 84%. Both the *T_G* and WII models have satisfactory prediction abilities, but the prediction accuracy of the WII model is 13% higher than that of the *T_G* model. The zones of water inrush risk derived from the *T_G* and WII models were compared. For 79% of the assessment samples, the prediction results from the *T_G* and WII models were the same and were mainly distributed in the northern areas where *T* is greater than 0.1 MPa/m and the southern areas where *T* is smaller than 0.06 MPa/m (Figs. 9 and 10; whereas for 21% of the samples, the *T_G* model and WII model predictions are the opposite. Forty-two assessment samples were classified as safe by the WII model, but these samples were classified as dangerous by the *T_G* model in the areas where $0.06 \le T < 0.10$ MPa/m (Fig. 9). In these areas, although the geological structure development degree is complex and the aquitard thickness is thin, the percentage of brittle rock within the aquitard is relatively high, indicating the strong mechanical strength of aquitards with complex geological structure development degree; thus, the aquifer water yield properties are poor (Fig. 8). By properly considering the influence of the mechanical strength of the aquitard and the water yield property, these 42 assessment samples were predicted to be safe from water inrush by the WII model, which was counter to the predictions from the *T_G* model. The remaining 61 assessment samples in areas where $T < 0.06$ MPa/m were classified as dangerous by the WII model, and safe by the *T_G* model (Fig. 9). The

Table 2 Comparison between the practical outcomes and the prediction results from the *T_G* and WII models

Test No.	*T* (MPa/m)	*G*	WII	Practice outcomes	Prediction by *T_G* model		Prediction by WII model	
					Result	Comparison to practice	Result	Comparison to practice
16	0.067	0.144	0.266	Safe	Dangerous	Disagree	Safe	Agree
17	0.066	0.154	0.266	Safe	Dangerous	Agree	Safe	Agree
22	0.035	0.142	0.213	Safe	Safe	Agree	Safe	Agree
29	0.067	0.186	0.262	Safe	Dangerous	Disagree	Safe	Agree
30	0.062	0.116	0.243	Safe	Safe	Agree	Safe	Agree
42	0.067	0.173	0.272	Safe	Dangerous	Disagree	Safe	Agree
57	0.077	0.186	0.305	Safe	Dangerous	Disagree	Safe	Agree
58	0.080	0.148	0.314	Safe	Dangerous	Disagree	Dangerous	Disagree
126	0.067	0.187	0.292	Safe	Dangerous	Disagree	Safe	Agree
139	0.057	0.100	0.259	Safe	Safe	Agree	Safe	Agree
140	0.067	0.169	0.288	Safe	Dangerous	Disagree	Safe	Agree
154	0.062	0.225	0.298	Safe	Dangerous	Disagree	Safe	Agree
155	0.077	0.220	0.329	Safe	Dangerous	Disagree	Dangerous	Disagree
213	0.012	0.100	0.304	Safe	Safe	Agree	Safe	Agree
214	0.015	0.110	0.304	Safe	Safe	Agree	Safe	Agree
215	0.015	0.116	0.305	Safe	Safe	Agree	Safe	Agree
225	0.010	0.095	0.299	Safe	Safe	Agree	Safe	Agree
226	0.013	0.097	0.299	Safe	Safe	Agree	Safe	Agree
227	0.017	0.112	0.303	Safe	Safe	Agree	Safe	Agree
228	0.025	0.157	0.297	Safe	Safe	Agree	Safe	Agree
229	0.040	0.207	0.305	Safe	Safe	Agree	Safe	Agree
238	0.013	0.096	0.298	Safe	Safe	Agree	Safe	Agree
239	0.018	0.101	0.297	Safe	Safe	Agree	Safe	Agree
249	0.013	0.097	0.272	Safe	Safe	Agree	Safe	Agree
250	0.019	0.112	0.281	Safe	Safe	Agree	Safe	Agree
261	0.018	0.101	0.268	Safe	Safe	Agree	Safe	Agree
262	0.023	0.167	0.304	Safe	Safe	Agree	Safe	Agree
271	0.016	0.109	0.257	Safe	Safe	Agree	Safe	Agree
272	0.022	0.148	0.273	Safe	Safe	Agree	Safe	Agree
281	0.013	0.100	0.235	Safe	Safe	Agree	Safe	Agree
282	0.020	0.129	0.251	Safe	Safe	Agree	Safe	Agree
289	0.011	0.102	0.226	Safe	Safe	Agree	Safe	Agree
290	0.021	0.124	0.245	Safe	Safe	Agree	Safe	Agree
358	0.018	0.086	0.168	Safe	Safe	Agree	Safe	Agree
359	0.030	0.100	0.189	Safe	Safe	Agree	Safe	Agree
365	0.013	0.095	0.172	Safe	Safe	Agree	Safe	Agree
366	0.023	0.100	0.183	Safe	Safe	Agree	Safe	Agree
367	0.037	0.148	0.221	Safe	Safe	Agree	Safe	Agree
373	0.015	0.102	0.181	Safe	Safe	Agree	Safe	Agree
374	0.026	0.108	0.193	Safe	Safe	Agree	Safe	Agree
375	0.039	0.140	0.227	Safe	Safe	Agree	Safe	Agree
381	0.015	0.097	0.187	Safe	Safe	Agree	Safe	Agree
391	0.022	0.103	0.203	Safe	Safe	Agree	Safe	Agree
392	0.032	0.101	0.210	Safe	Safe	Agree	Safe	Agree
400	0.026	0.153	0.221	Safe	Safe	Agree	Safe	Agree
412	0.041	0.182	0.243	Safe	Safe	Agree	Safe	Agree
413	0.047	0.129	0.238	Safe	Safe	Agree	Safe	Agree

Table 2 (continued)

Test No.	T (MPa/m)	G	WII	Practice outcomes	Prediction by T_G model		Prediction by WII model	
					Result	Comparison to practice	Result	Comparison to practice
414	0.054	0.169	0.259	Safe	Safe	Agree	Safe	Agree
415	0.061	0.207	0.281	Safe	Dangerous	Disagree	Safe	Agree
419	0.017	0.179	0.220	Safe	Safe	Agree	Safe	Agree
420	0.023	0.196	0.221	Safe	Safe	Agree	Safe	Agree
421	0.028	0.196	0.222	Safe	Safe	Agree	Safe	Agree
422	0.033	0.175	0.222	Safe	Safe	Agree	Safe	Agree
423	0.039	0.150	0.224	Safe	Safe	Agree	Safe	Agree
424	0.046	0.139	0.232	Safe	Safe	Agree	Safe	Agree
425	0.053	0.153	0.248	Safe	Safe	Agree	Safe	Agree
431	0.019	0.161	0.204	Safe	Safe	Agree	Safe	Agree
432	0.023	0.136	0.189	Safe	Safe	Agree	Safe	Agree
433	0.027	0.177	0.202	Safe	Safe	Agree	Safe	Agree
434	0.033	0.186	0.214	Safe	Safe	Agree	Safe	Agree
435	0.040	0.150	0.217	Safe	Safe	Agree	Safe	Agree
442	0.016	0.154	0.206	Safe	Safe	Agree	Safe	Agree
443	0.020	0.169	0.203	Safe	Safe	Agree	Safe	Agree
444	0.023	0.213	0.202	Safe	Safe	Agree	Safe	Agree
445	0.028	0.241	0.223	Safe	Safe	Agree	Safe	Agree
454	0.014	0.150	0.247	Safe	Safe	Agree	Safe	Agree
455	0.018	0.178	0.254	Safe	Safe	Agree	Safe	Agree
456	0.021	0.237	0.269	Safe	Safe	Agree	Safe	Agree
457	0.026	0.329	0.298	Safe	Safe	Agree	Safe	Agree
458	0.031	0.248	0.278	Safe	Safe	Agree	Safe	Agree
T1	0.070	0.328	0.306	Water inrush	Dangerous	Agree	Dangerous	Agree
T2	0.068	0.353	0.344	Water inrush	Dangerous	Agree	Dangerous	Agree
T3	0.051	0.267	0.306	Water inrush	Safe	Disagree	Dangerous	Agree
T4	0.061	0.318	0.335	Water inrush	Dangerous	Agree	Dangerous	Agree

reasons for these results are that the water resistance of an aquitard with a thin thickness and low percentage of brittle rock is low and the water yield property is rich in these areas, but the water pressure and C_p values are small (Fig. 8).

Based on the validation, a risk assessment of coal floor water inrush based on the T_G model and WII model is satisfactory. However, according to the comparative analysis of the predictions from these two methods, approximately 21% of the

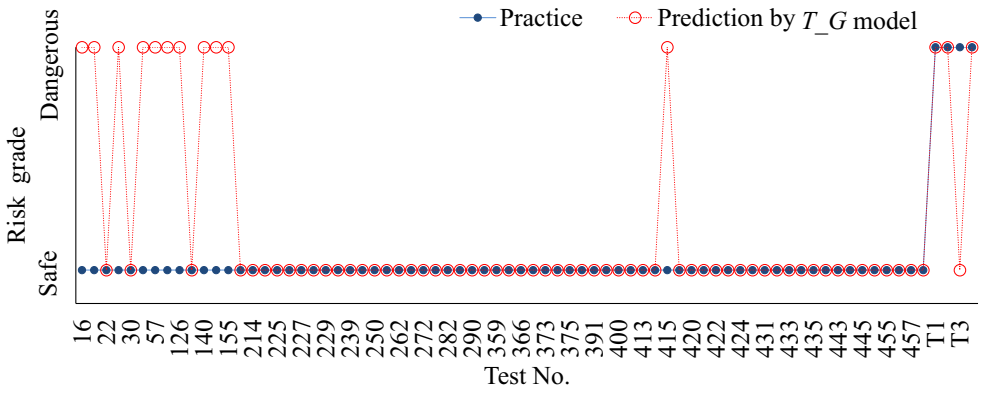

Fig. 11 Comparison between the practice outcomes and prediction results by the T_G model

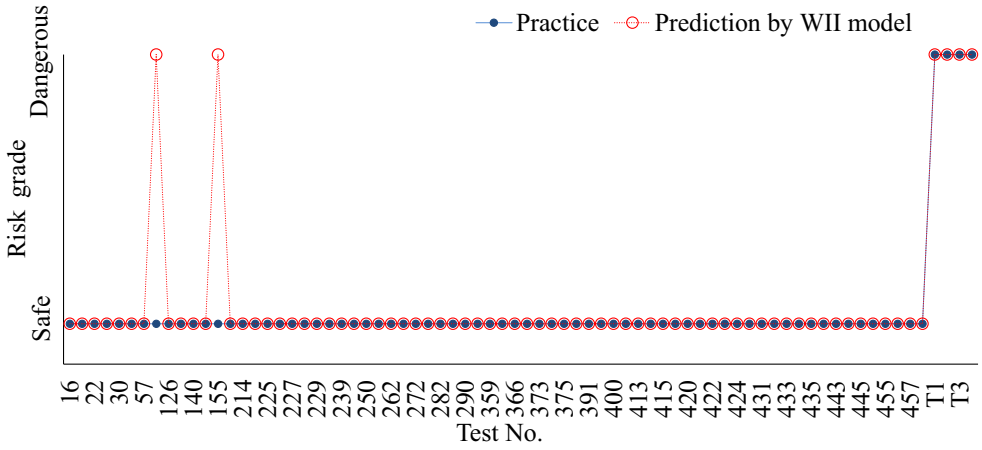

Fig. 12 Comparison between the practical outcomes and the prediction results from the WII model

predictions were not in agreement; therefore, more reasonable predictions can be achieved by combining the predictions from the *T_G* and WII models. The comprehensive application of the predictions from the *T_G* and *WII* models was proposed to evaluate the risk of water inrush from an underlying aquifer and used to divide the water inrush risk from an underlying aquifer into two zones and two subzones, as shown in Fig. 13.

1. Zone I: safe zone predicted by both the *T_G* and WII models, mainly distributed in the southeastern part and small parts of southwestern part in the study area.
2. Zone II: dangerous zone where at least one of the model predictions was dangerous and this zone was divided into two subzones:
   a. Zone II-1: a relatively dangerous zone that is a transition zone between a safe zone and an extremely dangerous zone.
   b. Zone II-2: extremely dangerous zone where predictions from both the *T_G* and WII models were dangerous; this zone type was mainly located in the northwestern part and small parts of the southwestern part in the study area.

The water-inrush risk zone map (Fig. 13) created after comprehensive application of the predictions from the *T_G* and WII models offers guidance on preventive measures necessary in the study area. Different preventive measures against water hazards associated with the underlying Ordovician limestone are proposed for the different zones as follows:

1. Safe zones: Monitor and investigate. The changes in inflow and aquifer water level variations must be monitored. Second, investigations on geological structures in the Ordovician limestone aquifer should be carried out. However, exposure of water-conductive geologic structures should be avoided and impermeable coal pillars should be retained based on the Coal Mine Water Control Rules (Ministry of Coal Industry 2018).
2. Relatively dangerous zones: These zones must be monitored and investigated. Additionally, impermeable coal pillars should be retained, as in the safe zones, and abnormal observations should be reported in a timely manner. Second, the weak zone of the aquitard, the water properties of the Ordovician limestone aquifer, and the potential of water-conducting faults should be explored by drilling, geophysical exploration and other means. If indications

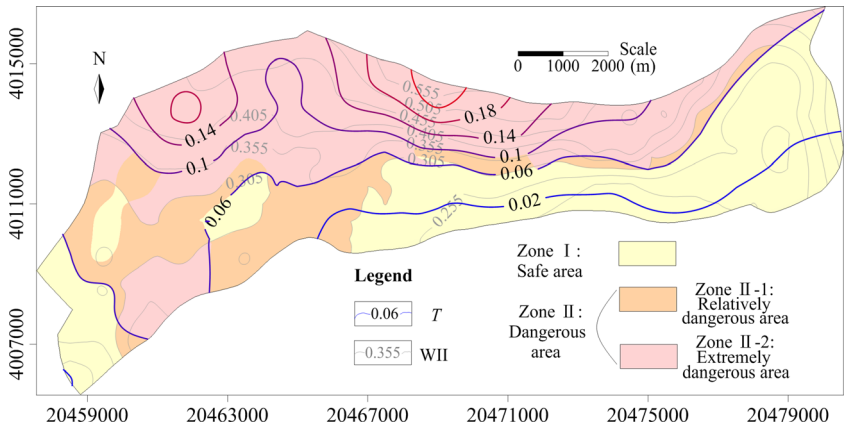

Fig. 13 Water-inrush risk zones by comprehensive application of the predictions from the *T_G* and WII models

are found, advanced grouting should be performed in water-rich areas, structural weak zones, and weak aquitards with thin thicknesses and low percentages of brittle rock.

3. Extremely dangerous zones: In addition to the conventional measures used in relatively dangerous zones, grouting should be used at the mining face, in conjunction with a drainage method. Pregrouting reinforcement of floor strata should be performed to strengthen and improve floor strata and the top of Ordovician limestone, to change the Ordovician top aquifer into a relatively water-resistant strata and to minimize the water inrush risk.

Conclusions

1. Water inrush from an underlying aquifer is a prominent problem threatening coal mine safety. It is essential but challenging to assess the risk of water inrush from an underlying aquifer. The *T_G* and WII models were comprehensively applied to refine the water-inrush risk zones in the No. 8 coal seam from the Ordovician limestone aquifer in Feicheng coalfield, China. The *T_G* model improved the traditional water-inrush coefficient method by quantifying the geological structure development degree, which considers three main controlling factors: *P*, *M*, and *G*. Based on the *T_G* model, the study area was divided into two zones: safe zones where $T < 0.06$ MPa/m or $0.06 \le T < 0.10$ MPa/m and $G < 0.137$, which were mainly distributed in the southern part and small southwestern part of the study area, and dangerous zones where $T \ge 0.10$ MPa/m or $0.06 \le T < 0.10$ MPa/m and $G \ge 0.137$, which were mainly located in the western and northern areas of the study area. Meanwhile, the WII model was constructed to assess the risk of floor water inrush by EWM, which integrated six factors, including *P*, *M*, C_p, *G*, *Y*, and *B*. The predicted water-inrush risk zones were divided into two zones: safe zones (WII < 0.305), mainly in the east, south, and southwest; and dangerous zones (WII ≥ 0.305), mainly in a small part of the western, northwestern, and northern parts of the study area.
2. Validation results from an analysis of the engineering practices showed that the risk assessment of a coal floor water inrush based on the *T_G* model and WII model is satisfactory. Based on the comparative analysis of predictions from these two models, the prediction accuracy of the WII model is 13% higher than that of the *T_G* model, and approximately 21% of the model predictions were not in agreement, which is partly because the *T_G* model neglects the influence of the aquifer water yield property, the depth of broken rock created by ground pressure and the percentage of brittle rock within the aquitard on water inrush, and also because the classification rules are different. Inevitably, the prediction quality of the methods should be further improved as more data are added.
3. A more reasonable prediction was finally accomplished by comprehensive application of the predictions from the *T_G* model and WII model to evaluate the risk of water inrush from an underlying aquifer. The comprehensive application of these two models allowed subdivision of the study area into two zones and two subzones, offering guidance on different preventive measures against water hazards in the underlying Ordovician limestone in the different zones.

Funding information We gratefully acknowledge the financial support of the National Natural Science Foundation of China (51804184, 41572244), the Scientific Research Foundation of Shandong University of Science and Technology for Recruited Talents (2017RCJJ033), the Open Fund Research Project of State Key Laboratory of Mining Disaster Prevention and Control Co-founded by Shandong Province and the Ministry of Science and Technology (MDPC2017ZR05), and the Shandong Province Nature Science Fund (ZR2015DM013).

References

Chang CW, Wu CR, Lin CT, Chen HC (2007) An application of AHP and sensitivity analysis for selecting the best slicing machine. Comput Ind Eng 52(2):296–307

Gu X, Wang J, Liu Y (2010) Water resistant features of high-risk outburst coal seams and standard discriminant model of mining under water-pressure. Min Sci Technol 20:0797–0802

Huang S, Ming B, Huang Q, Leng G, Hou B (2017) A case study on a combination NDVI forecasting model based on the entropy weight method. Water Resour Manag 31:3667–3681. https://doi.org/10.1007/s11269-017-1692-8

Li J (2000) The relations of in-situ rock stress and water-resisting ability for floor aquifuge. Coal Geology & Exploration 28(4):47–49

Li W, Liu Y, Qiao W, Zhao C, Yang D, Guo Q (2018) An improved vulnerability assessment model for floor water bursting from a confined aquifer based on the water inrush coefficient method. Mine Water Environ 37:196–204. https://doi.org/10.1007/s10230-017-0463-3

Ma L (2003) Standardization of statistical data-dimensionless method. Beijing Stat 3:34–35

Meng Z, Li G, Xie X (2012) A geological assessment method of floor water inrush risk and its application. Eng Geol 143–144:51–60. https://doi.org/10.1016/j.enggeo.2012.06.004

Ministry of Coal Industry (2009) Regulations for coal mine water prevention and control. China Coal Industry Publ. House, Beijing

Ministry of Coal Industry (2018) Coal mine water control rules. China Coal Industry Publ. House, Beijing

National Bureau of Coal Industry of China (2000) Pillar design and mining regulations under buildings, water, rails and major roadways. China Coal Industry Publ. House, Beijing

Qiu M (2016) Karst development and grouting reinforcement of Ordovician top in Feicheng coalfield. PhD Thesis, Qingdao University, Qingdao, China

Qiu M, Han J, Zhou Y, Shi LQ (2017a) Prediction reliability of water inrush through the coal mine floor. Mine Water Environ 36(2):217–225. https://doi.org/10.1007/s10230-017-0431-y

Qiu M, Shi LQ, Teng C, Zhou Y (2017b) Assessment of water inrush risk using the fuzzy Delphi analytic hierarchy process and Grey relational analysis in the Liangzhuang coal mine, China. Mine Water Environ 36(1):39–50. https://doi.org/10.1007/s10230-016-0391-7

Saaty TL (1980) The analytic hierarchy process. McGraw-Hill, New York

Shannon CE (1948) A Mathematical Theory of Communication. Bell System Technical Journal 27(4):623-656

Shi L, Gao W, Han J, Tan X (2017) A nonlinear risk evaluation method for water inrush through the seam floor. Mine Water Environ 36(4): 597–605. https://doi.org/10.1007/s10230-017-0449-1

Shi LQ, Bo CS, Wei JC (2015) Control theory and technology of Ordovician limestone karst water inrush in North China coalfield. China Coal Industry Publ. House, Beijing

Sun W, Wu Q, Liu H, Jiao J (2015) Prediction and assessment of the disturbances of the coal mining in Kailuan to karst groundwater system. Phys Chem Earth 89–90:136–144

Wang Y, Yang W, Li M, Liu X (2012) Risk assessment of floor water inrush in coal mines based on secondary fuzzy comprehensive evaluation. Int J Rock Mech Min Sci 52:50–55. https://doi.org/10.1016/j.ijrmms.2012.03.006

Wang Z, Wang C, Wang Z (2018) The hazard analysis of water inrush of mining of thick coal seam under reservoir based on entropy weight evaluation method. Geotech Geol Eng 36(5):3019–3028. https://doi.org/10.1007/s10706-018-0520-0

Wu J, Li P, Qian H, Chen J (2015) On the sensitivity of entropy weight to sample statistics in assessing water quality: statistical analysis based on large stochastic samples. Environ Earth Sci 74:2185–2195. https://doi.org/10.1007/s12665-015-4208-y

Wu Q, Zhou W (2008) Prediction of groundwater inrush into coal mines from aquifers underlying the coal seams in China: vulnerability index method and its construction. Environ Geol 55(4):245–254. https://doi.org/10.1007/s00254-007-1160-5

Wu Q, Xie S, Pei Z, Ma J (2007) A new practical methodology of the coal floor water bursting evaluating III: the application of ANN vulnerable index method based on GIS. J China Coal Soc 32(12):1301–1306

Wu Q, Xu H, Pang W (2008) GIS and ANN coupling model: an innovative approach to evaluate vulnerability of karst water inrush in coalmines of North China. Environ Geol 54:937–943. https://doi.org/10.1007/s00254-007-0887-3

Wu Q, Liu Y, Liu D, Zhou W (2011) Prediction of floor water inrush: the application of GIS-based AHP vulnerable index method to Donghuantuo coal mine, China. Rock Mech Rock Eng 44:591–600. https://doi.org/10.1007/s00603-011-0146-5

Wu Q, Zhao D, Wang Y, Shen J, Mu W (2017) Method for assessing coal-floor water-inrush risk based on the variable-weight model and unascertained measure theory. Hydrogeol J 25:2089–2103. https://doi.org/10.1007/s10040-017-1614-0

Xu F, Long R, Xia Y, Xie S (1991) Quantitative assessment and prediction of geological structures in coal mine. J China Coal Soc 16(4): 93–102

Zhao D, Wu Q, Cui F, Xu H, Zeng Y, Cao Y, Du Y (2018) Using random forest for the risk assessment of coal-floor water inrush in Panjiayao coal mine, northern China. Hydrogeol J 26(7):2327–2340. https://doi.org/10.1007/s10040-018-1767-5